Structure of Self-Organized Multilayer Nanoparticles for Drug Delivery

ARTICLE *in* LANGMUIR · OCTOBER 2008

Impact Factor: 4.46 · DOI: 10.1021/la801992t · Source: PubMed

Structure of Self-Organized Multilayer Nanoparticles for Drug Delivery

Y. Gerelli,[†] S. Barbieri,[‡] M. T. Di Bari,[†] A. Deriu,[†,*] L. Cantù,[§] P. Brocca,[§] F. Sonvico,[‡] P. Colombo,[‡] R. May,[||] and S. Motta[‡]

Dipartimento di Fisica, Università degli Studi di Parma and CNISM, CRS SOFT, INFM-CNR, Parma, Italy, Dipartimento di Chimica, Biochimica e Biotecnologie per la Medicina−LITA, Università di Milano and CNISM, Milano, Italy, Dipartimento Farmaceutico, Università degli Studi di Parma, Parma, Italy, and Institut Laue-Langevin, Grenoble, France

Received June 25, 2008. Revised Manuscript Received July 31, 2008

The combined use of cryo-TEM, dynamic light scattering, and small-angle X-ray and neutron scattering techniques allows a detailed structural model of complex pharmaceutical preparations of soybean lecithin/chitosan nanoparticles used as drug vectors to be worked out. Charge-driven self-organization of the lipid(−)/polysaccharide(+) vesicles occurs during rapid injection, under mechanical stirring, of an ethanol solution of soybean lecithin into a chitosan aqueous solution. We conclude that beyond the charge inversion region of the phase diagram, i.e., entering the redissolution region, the initial stages of particle formation are likely to be affected by a re-entrant condensation effect at the nanoscale. This behavior resembles that at the mesoscale which is well-known for polyion/amphiphile systems. Close to the boundary of the charge inversion region, nanoparticle formation occurs under a maximum condensation condition at the nanoscale and the complexation−aggregation process is driven toward a maximum multilamellarity. Interestingly, the formulation that maximizes vesicle multilamellarity corresponds to that displaying the highest drug loading efficiency.

Introduction

In health care and pharmaceutical sciences, nanotechnologies have been indicated as the most promising field for breakthrough technological innovation in early disease diagnosis and in improved therapies. In recent years, nanotechnologies have been proposed to improve drug delivery: specific nanovectors capable of carrying the biologically active principle have been developed to protect the encapsulated drug and to modify its distribution, altering the pharmacokinetics.[1,2] In pharmaceutical nanotechnologies, colloidal carriers are considered particularly suited for the administration of drugs with biopharmaceutical problems such as low bioavailability and poor water solubility. In this respect different nanosized systems have been proposed to improve drug bioavailability such as liposomes,[3] polymeric micelles,[4] and nanoemulsions and nanoparticles.[5,6] Some liposomal and nanoparticle vectors have already been approved for clinical application, in particular for cancer treatment, while several others are under evaluation.[7] Recently, great attention has been devoted to colloidal preparations employing lipid systems: as compared to synthetic polymers, these materials are considered more biocompatible, biodegradable, and safe.[8] In particular, films and gels based on negatively charged phospholipids and chitosan have been proposed for the delivery of poorly soluble anticancer drugs.[9,10]

In this work we address lipid/polysaccharide systems, involving lecithin and chitosan. Lecithin is a lipid mixture of phospholipids that has been frequently used for liposome and micelle formation[11,12] and is largely employed in pharmaceutical or nutraceutical formulations. The basic structure of lecithin-based nanovesicles is common to all membrane-like amphiphile aggregates;[13] however, their stability, physicochemical properties, and surface characteristics need to be tailored to control the release of the trapped drug, to adapt the nanocarrier to different chemical environments, and to direct the nanocarrier toward specific biological targets. In particular, the surface properties of nanocarriers are important for their interaction with living systems; they can be modified using both synthetic[6,14] and natural[15,16] polymers. Several polysaccharides have been investigated for the stabilization of lipid membranes. Among them, chitosan, a cationic polysaccharide derived from chitin by deacetylation, has emerged because of its favorable biochemical characteristics, including low toxicity, high biocompatibility, biodegradability, bioadhesion, and absorption enhancer properties.[17,18] Chitosan has been used for the production of nanoparticles by ionotropic gelation with tripolyphosphate[19,20] as well

* To whom correspondence should be addressed. E-mail: Antonio.Deriu@fis.unipr.it. Phone: +39 0521 905267. Fax: +39 0521 905223.

[†] Dipartimento di Fisica, Università degli Studi di Parma and CNISM, CRS SOFT, INFM-CNR.

[‡] Università di Milano and CNISM.

[§] Dipartimento Farmaceutico, Università degli Studi di Parma.

[||] Institut Laue-Langevin.

(1) Hughes, G. A. *Nanomedicine* **2005**, *1*, 22–30.

(2) Oh, K. S.; Han, S. K.; Lee, H. S.; Koo, H. M.; Kim, R. S.; Lee, K. E.; Han, S. S.; Cho, S. H.; Yuk, S. H. *Biomacromolecules* **2006**, *7*, 2362–2367.

(3) Malzert-Fréon, A.; Vrignaud, S.; Saulnier, P.; Lisowski, V.; Benoît, J. P.; Rault, S. *Int. J. Pharm.* **2006**, *320*, 157–164.

(4) Jones, M. C.; Leroux, J. C. *Eur. J. Pharm. Biopharm.* **1999**, *48*, 101–111.

(5) Sonvico, F.; Cagnani, A.; Rossi, A.; Motta, S.; Di Bari, M. T.; Cavatorta, F.; Alonso, M. J.; Deriu, A.; Colombo, P. *Int. J. Pharm.* **2006**, *324*, 67–73.

(6) Teng, X. R.; Shchukin, D. G.; Mohwald, H. *Langmuir* **2008**, *24*, 383–389.

(7) Torchilin, V. P. *Nat. Rev. Drug Discovery* **2005**, *4*, 145–160.

(8) Igarashi, R.; Takenaga, M.; Matsuda, T. *Adv. Drug Delivery Rev.* **1996**, *20*, 147–154.

(9) Grant, J.; Blicker, M.; Piquette-Miller, M.; Allen, C. *J. Pharm. Sci.* **2005**, *94*, 1512–1527.

(10) Ho, E. A.; Vassileva, V.; Allen, C.; Piquette-Miller, M. *J. Controlled Release* **2005**, *104*, 181–191.

(11) Batzri, S.; Korn, E. D. *Biochim. Biophys. Acta* **1973**, *298*, 1015–1019.

(12) Betageri, G. V.; Jenkins, S. A.; Parsons, D. L. *Liposome Drug Delivery Systems*; Technomic Publishing: Lancaster, PA, 1993.

(13) Imura, T.; Otake, K.; Hashimoto, S.; Gotoh, T.; Yuasa, M.; Yokoyama, S.; Sakai, H.; Rathman, J. F.; Abe, M. *Colloids Surf., B* **2003**, *27*, 133–140.

(14) Johnsson, M.; Bergstrand, N.; Edwards, K.; Stålgren, J. J. R. *Langmuir* **2001**, *17*, 3902–3911.

(15) Lemp, E.; Zanocco, A. L.; Günther, G. *Colloids Surf., A* **2003**, *229*, 63–73.

(16) Perugini, P.; Genta, I.; Pavanetto, F.; Conti, B.; Scalia, S.; Baruffini, A. *Int. J. Pharm.* **2000**, *196*, 51–61.

10.1021/la801992t CCC: $40.75
Published on Web 09/24/2008

as for improving the stability of lecithin-based microemulsions.[21,22] Interestingly, the "coating" of these lipid-based nanostructures with chitosan, besides increasing their stability,[23,24] provides them with mucoadhesion properties[25] and enhances permeation because of its effect of tight junctions between cells. Thus, lecithin/chitosan nanoparticles are promising carriers for the delivery of drugs via tranmucosal routes, such as oral, nasal, or pulmonary administration.

The physical context in which the complexation mechanism between lecithin and chitosan can be placed is that of macroion−polyion interactions. Particular attention has been devoted to complexes formed by lipid vesicles incubated with polyions, adhering to their surfaces and giving rise to ordered patterns or coordinating different vesicles. A rich literature exists on complex structures consisting of amphiphile aggregates interacting via electrostatic forces with linear polyions, polypeptides, or DNA, including lamellar phases or dispersed particles.[26,27] A characterizing feature of the phase behavior of such systems is charge inversion, corresponding to oppositely charge polyelectrolytes complexing beyond charge neutralization. Amphiphile/polyion coordination reaches its maximum in the region of charge inversion where large clusters are formed. This behavior can be described in terms of a re-entrant condensation effect: extra polyions can be attracted to the surface of the macroion despite the fact that this surface is already neutralized by the previously adsorbed polyions. This entropically driven process is due to an induced attraction between polyions.[28] In the present work we address the complexation mechanism between the macroion and polyions at the nanoscale and their role in determining the ultimate structure of the nanoparticles. To this purpose the lecithin/chitosan nanoparticles described in this paper were obtained by direct injection of a soybean lecithin alcoholic solution into a chitosan/water solution. The nanoparticle supramolecular self-organization is contemporarily driven by the aggregative behavior of the lipid component and by the electrostatic interaction between the negatively charged fraction of the lipid material and the positively charged polysaccharide. A detailed morphological and structural characterization of the nanoparticle, as a function of the chitosan content in the initial chitosan/water preparation solution, is essential to optimize the loading efficiency and to tune the drug release kinetics. Selected formulations spanning the phase diagram, before and after the demixing region[5] and deep in the re-entrant condensation range, were chosen for this study. The nanovectors were initially characterized by cryo-TEM (cTEM), dynamic light scattering (DLS), and surface charge determination (ζ potential). Small-angle X-ray scattering (SAXS) and small-angle neutron scattering (SANS) experiments were then performed.

Experimental Section

Sample Preparation. The investigated nanoparticles are made up of two main components. One is Lipoid S45 (a lecithin manufactured by Lipoid AG, Switzerland), a commercial mixture of lipids, phospholipids, and fatty acids with an overall negative charge and with the following composition: (lipid components) phosphatidylcoline, 47.6%; phosphatidylethanolamine, 16.4%; lysophosphatidylcoline, 2.5%; (acid components) palmitic acid, 15%; stearic acid, 3%; oleic acid and isomers, 12%; linoleic acid, 5%; (other minor components) tryriglycerides, 0.1%; DL-α-tocopherol, 0.10%; water (Karl Fisher), 0.6%; ethanol, 0.5%. The other is highly purified chitosan (provided by Primex, Norway), a polysaccharide, positively charged at acidic pH, obtained by deacetylation of chitin. Its average molecular weight, as determined by laser light scattering, is ∼140 000. The samples were prepared from a lecithin solution (lecithin in ethanol at 25 mg/mL concentration) and from three different chitosan/water solutions (chitosan/lecithin ratios 1/80, 1/20, and 1/5 (w/w), acidic pH). When necessary, as for laser light scattering measurements, solvents were filtered on 0.2 μm polycarbonate membranes before nanoparticle preparation; filtration of the final solutions was avoided. The samples obtained from these starting formulations are indicated in the following as NCL80, NCL20, and NCL5. Self-assembled nanoparticles were obtained by rapid injection (nozzle diameter 0.75 mm, injection rate 40 mL/min), under mechanical stirring, of the ethanol solution into the chitosan aqueous solution. The self-assembly process gave rise to a suspension with a pH of 2.7 and a nanoparticle concentration $c = 0.2\%$ (w/w).[5] Lipoid vesicles, used as a reference for the SAXS measurements, were prepared with a similar procedure, replacing the chitosan/water solution with water, acidic pH.

The residual chitosan content in the buffer, after nanoparticle formation, was determined by a colorimetric method, on the basis of the $\lambda = 581$ nm absorbance of the sample solution, upon addition of Cibacron Brillant Red 3B-A (Sigma, St.Louis, MO)[29] as a specific dye. SAXS measurements of chitosan in H_2O/HCl solution (pH 2.7) were performed at three different concentrations (0.02%, 0.1%, and 1%).

Cryo-Tem. The nanoparticle morphology was investigated by electron transmission microscopy on thin (∼5000 Å) aqueous films vitrified by cooling to liquid nitrogen temperature (cTEM).[30] The limiting factor, when using electrons as probes, is the small difference between the electron density of the lipids and that of the aqueous solvent. As a consequence the spatial resolution cannot be higher than ∼40−50 Å. This corresponds to a typical bilayer thickness; therefore, the internal structure of the bilayers and other smaller scale details cannot be resolved by this technique.

Dynamic Laser Light Scattering. The particle size distribution was determined by DLS using a 200SM apparatus (Brookhaven Instruments Corp.), equipped with an argon ion laser operating on the 5145 Å green line; the accessible Q range is 4×10^{-4}−3×10^{-3} Å^{-1}. As compared to the other adopted techniques, DLS is the only one looking at the dynamics of the nanoparticles in Brownian motion in the solution, rather than at their "static" average scattered intensity.

The average charge of the nanoparticles is expressed in terms of the ζ potential[31] as obtained from a measure of their mobility under an electric field with a ZetaPals phase analysis light scattering apparatus (Brookhaven Instruments Corp.).

Small-Angle X-Ray Scattering. SAXS data were collected at the ID02 beamline at the European Synchrotron Radiation Facility, ESRF (Grenoble). Using a wavelength $\lambda = 1$ Å (instrument resolution $\Delta E/E = 2 \times 10^{-4}$) and a sample−detector distance $D = 1.2$ m, a Q range from 8×10^{-3} to 4×10^{-1} Å^{-1} was explored corresponding to a range of length scales from 15 to 800 Å. The particle structure down to the bilayer length scale is accessible by this technique. Calibration was performed using a silver behenate standard. The

(17) Ilium, L. *Pharm. Res.* **1998**, *15*, 1326–1331.
(18) Singla, A. K.; Chawla, M. *J. Pharm. Pharmacol.* **2001**, *53*, 1047–1067.
(19) Agnihotri, S. A.; Mallikarjuna, N. N.; Aminabhavi, T. M. *J. Controlled Release* **2004**, *100*, 5–28.
(20) Janes, K. A.; Calvo, P.; Alonso, M. J. *Adv. Drug Delivery Rev.* **2001**, *47*, 83–97.
(21) Alonso, F. M. J.; Calvo, S. P.; Remunan, L. C.; Vila, J. J. L. Stabilization of Colloidal Systems by the Formation of Ionic Lipid-Polysaccharide Complexes. EP0771566, 1997.
(22) Calvo, P.; Remunan-Lopez, C.; Vila-Jato, J. L.; Alonso, M. J. *J. Appl. Polym. Sci.* **1997**, *63*, 125–132.
(23) Henriksen, I.; Smistad, G.; Karlsen, J. *Int. J. Pharm.* **1994**, *101*, 227–236.
(24) Henriksen, I.; Vågen, S. R.; Sande, S. A.; Smistad, G.; Karlsen, J. *Int. J. Pharm.* **1997**, *146*, 193–203.
(25) Takeuchi, H.; Matsui, Y.; Yamamoto, H.; Kawashima, Y. *J. Controlled Release* **2003**, *86*, 235–242.
(26) Sennato, S.; Bordi, F.; Cametti, C.; Marianecci, C.; Carafa, M.; Cametti, M. *J. Phys. Chem. B* **2008**, *112*, 3720–3727.
(27) Koltover, I.; Salditt, T.; Safinya, C. R. *Biophys. J.* **1999**, *77*, 915–924.
(28) Grosberg, A. Y.; Nguyen, T. T.; Shklovskii, B. I. *Rev. Mod. Phys.* **2002**, *74*, 329–345.
(29) Muzzarelli, R. A. A. *Anal. Biochem.* **1998**, *260*, 255–257.
(30) Almgren, M.; Edwards, K.; Karlsson, G. *Colloids Surf., A* **2000**, *174*, 3–21.
(31) Hunter, R. J. *Zeta Potential in Colloid Science: Principles and Applications*; Academic Press: New York, 1981.

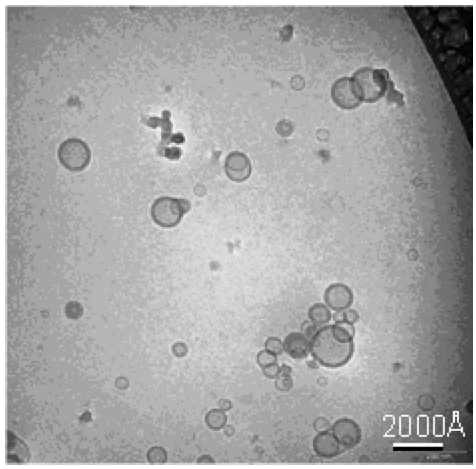

Figure 1. cTEM micrograph of an NLC20 sample. All nanoparticles have a large core surrounded by an external layer of variable thickness. Nanoparticle polydispersity is evident, as well as the presence of particle clusters with variable size.

scattering profiles were processed and corrected with the ID02 software; background subtraction was performed at a later stage.

Small-Angle Neutron Scattering. SANS experiments were performed at the Institut Laue-Langevin, ILL (Grenoble), using the D11 diffractometer. To cover a Q range of about 2 decades from 1×10^{-3} to 0.1 Å^{-1} (length scale from 60 to 6000 Å), three different instrument configurations were adopted with the following wavelength and sample−detector distance combinations: $\lambda = 5$ Å, $D = 5.5$ m; $\lambda = 5$ Å, $D = 20.5$ m; $\lambda = 10$ Å, $D = 34$ m. Sample holders were standard quartz flat cells (1 mm thick). Standard corrections, cell subtraction, and normalization to absolute scattering units were performed using ILL SANS routines. The samples for the SANS experiments were prepared in two different buffers: a 100% D_2O solution and a 4/1 H_2O/D_2O mixture that almost matches the Lipoid coherent scattering signal.

Results

On the basis of the cTEM analysis, we describe the nanoparticle structure in terms of different populations: small nanoparticles with a single bilayer outer structure and large ones with a multilayer structure with a variable number, N, of bilayers. The mathematical derivations of the models adopted in this section to analyze DLS, SAXS, and SANS data are given in the Supporting Information.[32−37] For the sake of clarity, experimental results will be discussed in separated sections for the different techniques.

Colorimetry. The residual chitosan content in the buffer after the nanoparticle formations has been determined by colorimetry. It is close to zero for NCL80, ∼3% of the initial chitosan content for NCL20, and close to 70% of the initial chitosan content for NCL5. Therefore, due to the high electron density of sugar compounds, NCL5 SAXS data required an accurate subtraction of the scattering contribution of the residual chitosan. In the SANS case, this contribution can be ignored owing to the lower neutron contrast of saccharides with respect to that of X-rays.

Cryo-TEM Data. The cTEM data provide an overall picture of the nanoparticle morphology. Figure 1 shows typical micrographs for NCL20 samples. It can be seen that the thicker

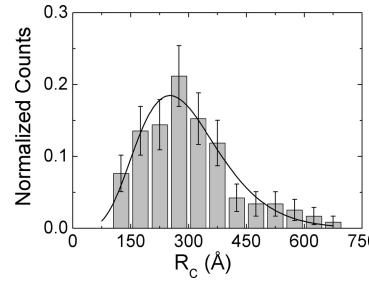

Figure 2. Hollow-core radius distribution for NCL20 samples derived from a computer analysis of the cTEM images (histogram). The continuous curve is a fit to a Schulz distribution with $\langle R_C \rangle = 310 \pm 30$ Å and a polydispersity index $\sigma = 0.39 \pm 0.03$.

outer shells are made up by the superposition of several layers; the outer ones sometimes wrap up two or more particles. It is also evident that the nanoparticles are polydisperse and that clusters with variable size are present. The existence of such clusters is expected in lipid/polyion systems; their size and number increase as the isoelectric point is approached.[38] A statistical image analysis performed on the cTEM micrograph provided information on the nanoparticle size distribution. To obtain the core radius distribution, we considered an ensemble of about 110 individual nanoparticles disregarding clusters. Due to the cTEM film deposition method forcing larger particles to the film boundary, this analysis can be affected by the choice of the region of observation.[39] For NCL20 particles (Figure 2), a reasonable fit can be obtained with a Schulz distribution with a mean core radius $\langle R_C \rangle = 310 \pm 30$ Å and a polydispersity index $\sigma = 0.39 \pm 0.03$.

DLS Data. The time correlation functions were collected at a 90° scattering angle ($Q = 2.3 \times 10^{-3}$ Å^{-1}). The analysis has been performed using an exponential sampling as well as a non-negatively constrained least-squares (NNLS) algorithm.[40] They both show that the nanoparticle distributions are markedly bimodal for all the investigated samples. As an example, the result for NCL20 samples is shown in Figure 3a. The number of nanoparticles in the larger size population is very low, although giving a huge contribution in intensity due to the quadratic molecular weight dependence of the scattering. The construction of a number-weighted distribution requires a structural assumption for the nanoparticles. Moreover, the large size aggregates are clearly identified with clusters of nanoparticles, also seen in the cTEM image. Figure 3b shows the field correlation function, $g_1(\tau)$, from which the distribution of Figure 3a is derived (upper curve). It can be analyzed in terms of two exponential decays. The lower curve in Figure 3b shows $g_1(\tau)$ after the subtraction of the long-time decay due to the nanoparticle clusters. It has been analyzed with the cumulant method (see the Supporting Information) to obtain the average hydrodynamic radius $\langle R_H \rangle$ and the polydispersity of the nanoparticle distribution. The same procedure has been followed for the NCL80 and NCL5 nanoparticles and for the lecithin vesicles. The obtained parameters are summarized in Table 1. The data in Table 1 indicate that chitosan addition leads to nanoparticles much larger than the vesicles obtained with Lipoid.

ζ Potential Data. The average charge per nanoparticle is negative for the lecithin vesicles, due to the anionic fraction of

(32) Koppel, D. E. *J. Chem. Phys.* **2003**, *57*, 4814.
(33) Nallet, F.; Laversanne, R.; Roux, D. *J. Phys. II* **1993**, *3*, 487–502.
(34) Chen, W. R.; Butler, P. D.; Magid, L. J. *Langmuir* **2006**, *22*, 6539–6548.
(35) Pedersen, J. S.; Schurtenberger, P. *Macromolecules* **1996**, *29*, 7602–7612.
(36) Kotlarchyk, M.; Stephens, R. B.; Huang, J. S. *J. Phys. Chem.* **1988**, *92*, 1533–1538.
(37) Cern Program Library. http://cerlib.web.cern.ch/cernlib/.
(38) Bordi, F.; Cametti, C.; Sennato, S. *Chem. Phys. Lett.* **2005**, *409*, 134–138.
(39) Egelhaaf, S. U.; Wehrli, E.; Muller, M.; Adrian, M.; Schurtenberger, P. *J. Microsc.* **1996**, *184*, 214–228.
(40) Grabowski, E.; Morrison, I. Measurements of Suspended Particles by Quasi-Elastic Light Scattering. In *Particle Size Distributions from Analysis of Quasi-Elastic Light Scattering Data*; Dahneke, B., Ed.; Wiley-Interscience: New York, 1983; Vol. *30*, pp 113−121.

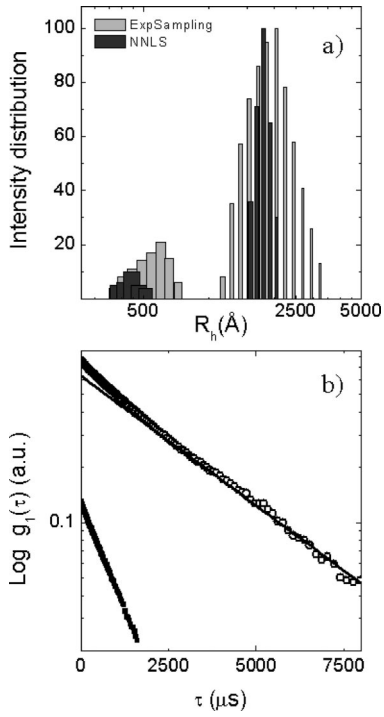

Figure 3. (a) Size distribution of the scattered laser light intensity, as determined by non-negatively constrained least-squares (gray) and by exponential sampling (white) analyses of the correlation function for NCL20 nanoparticle solutions. (b) Field correlation function for NCL20 nanoparticles (upper curve) and the same function after subtraction of the nanoparticle cluster contribution (lower curve).

Table 1. Weight-Average Hydrodynamic Radius $\langle R_H \rangle$ and Polydispersity σ of Lecithin Vesicles and Chitosan/Lecithin Nanoparticles, As Obtained by the Cumulant Analysis of the Laser Light Scattering Data Described in the Text

	lipid vesicles	NCL80	NCL20	NCL5
$\langle R_H \rangle$ (Å)	100 ± 5	1140 ± 50	650 ± 20	570 ± 20
σ (%)	23	56	40	20

the lipid mixture, and results in a negative ζ potential (-53 ± 1 mV). A decrease is expected upon addition of chitosan: for NCL80 samples (lowest chitosan content) we obtain -46 ± 2 mV, while for NCL20 and NCL5 samples the measured ζ potential is $+45 \pm 2$ and $+41 \pm 1$ mV, respectively. In fact, NCL80 and NCL20 lie on opposite sides of the miscibility gap of the Lipoid/chitosan system, covering the 50/1 to 30/1 range.[5] The ζ potential value of pure chitosan solution in the same pH condition is +40 mV. The colorimetry measurements indicate that for the NCL20 and NCL5 samples the amount of "free" chitosan in solution is 3% and 70%, respectively. The measured conductivities of the two samples are 0.32 and 1.2 S m^{-1}, respectively.

SAXS Data. *Lecithin.* The SAXS model adopted for the nanoparticles (Supporting Information, eq S.3) can be applied also to data from pure lecithin (Lipoid) vesicles if one assumes that the interbilayer regions are occupied only by the solvent (i.e., $\rho_{cw} - \rho_s = 0$). The results of the fits are shown in Table 2 and Figure 4. In the explored Q range, the individual contributions to the scattering intensity corresponding to $N = 1$ and 2 (mono- and bilamellar vesicles) cannot be distinguished. Therefore, the number fraction $g_1 + g_2$ takes into account both $N = 1$ and $N = 2$ populations. The $N = 3$ population contribution is clearly visible since it gives rise to an additional broad peak centered at $Q \approx 0.11$ Å^{-1}.

Since the commercial lecithin used in sample preparation (Lipoid S45) is a mixture of different lipid species, the use of a bilayer model more detailed[41,42] than the three strips adopted here is not justified. Moreover, reasonable criteria can be applied to this model considering that (a) the electron density of the hydrophobic region ρ_t is rather uniform over different lipids (in the fluid phase, 0.28 e/Å^3) and (b) the average surface area per lipid molecule can be assumed to be 55 Å^2, as in a fluid phase for the lipid chains. The parameters obtained from the fit of the lecithin scattering profile, reported in Table 2, are consistent, on average, with literature values for the main lipids present in the Lipoid composition. The values of ρ_t and ρ_h derived from the above analysis, as well as that of the molecular volume V_m, were then used as fixed input parameters during the analysis of the lecithin/chitosan nanoparticle data.

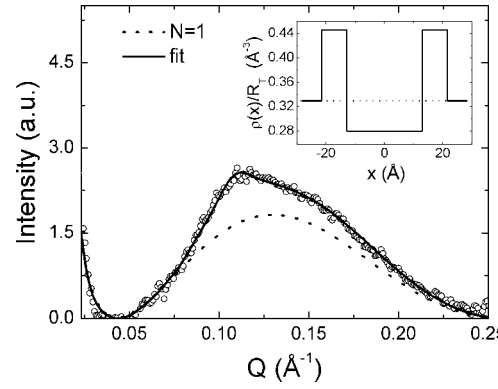

Figure 4. SAXS profile of pure lecithin vesicles. The total fit (solid line) is shown together with the form factor of the unilamellar vesicles (dashed line). The form factor of the multilamellar vesicles has been obtained by multiplying the form factor $P(Q)$ by the structure factor $S(Q,d,N_i)$ (Supporting Information, eqs S.1 and S.3). The inset shows the electron density profile across a bilayer; R_T is the Thomson scattering length.

Table 2. Fit Parameters Obtained by Applying Eq S.3 (Supporting Information) to SAXS Data on Lipid Vesicles[a]

$g_1 + g_2$ ($N = 1, 2$)	0.60 ± 0.03
g_3 ($N = 3$)	0.40 ± 0.03
t_t (Å)	13.0 ± 0.2
t_h (Å)	8.5 ± 0.2
ρ_h/R_T (Å^{-3})	0.446 ± 0.005

[a] R_T is the Thomson scattering length.

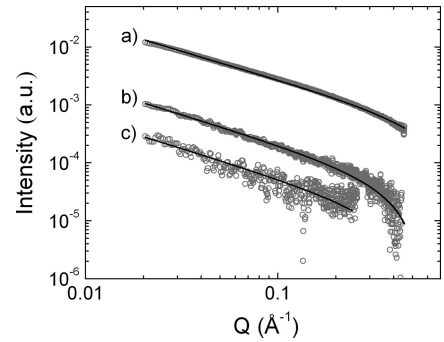

Figure 5. SAXS profiles of chitosan in acidic aqueous solution (pH 2.7) at three different concentrations: 1% (a), 0.1% (b), and 0.02% (c). The slope at intermediate Q values is -1, indicating an extended rodlike conformation.

Chitosan. In Figure 5 the scattered intensities obtained from chitosan aqueous solutions are shown for different concentrations. At acidic pH, chitosan chains are positively charged and adopt

(41) Kucerka, N.; Nagle, J. F.; Feller, S. E.; Balgavy, P. *Phys. Rev. E* **2004**, *69*, 51903.
(42) Kucerka, N.; Pencer, J.; Sachs, J. N.; Nagle, J. F.; Katsaras, J. *Langmuir* **2007**, *23*, 1292–1299.

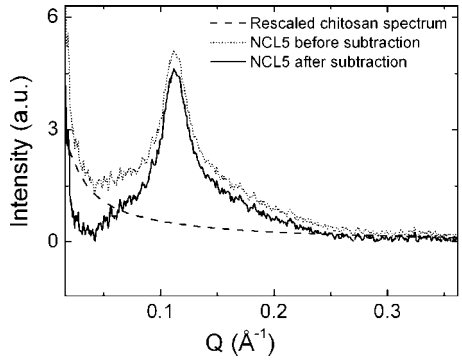

Figure 6. SAXS profiles of NCL5 before (dotted curve) and after (continuous curve) subtraction of the contribution due to residual chitosan molecules in the solution. The chitosan scattering intensity to be subtracted (dashed line) was rescaled according to the concentration of free chitosan determined by colorimetry.

Table 3. Parameters Obtained by Fitting SAXS Data of NCL Samples to Eq S.3 (Supporting Information)[a]

	NCL80	NCL20	NCL5
t_t (Å)	13.0 (12.8−13.1)	12.96 (12.6−13.2)	13.1 (12.8−13.2)
t_h (Å)	8.66 (8.5−8.8)	8.54 (8.4−8.8)	8.5 (8.4−8.8)
t_{cw} (Å)	12.0	12.1	12.6
α	0.04 ± 0.01	0.16 ± 0.01	0.126 ± 0.004
$g_1 + g_2$ ($N = 1, 2$)	0.84 ± 0.01	0.60 ± 0.01	0.86 ± 0.01
g_3 ($N = 3$)	0.13 ± 0.01	0.35 ± 0.01	0.12 ± 0.01
g_4 ($N > 3$)	0.03 ± 0.01 ($N = 11$)	0.05 ± 0.01 ($N = 7$)	0.05 ± 0.01 ($N = 7$)

[a] α is the volume fraction of chitosan in the interlayer region. Values in parentheses for t_t and t_h refer to results obtained by changing the lipid molecular volume by 7% and keeping the electron density constant.

an extended almost-straight conformation; this leads to the typical Q^{-1} power law. The average molecular weight, derived from light scattering data, is about 140 000, corresponding to roughly 860 repeating monomers and therefore to an overall length of the extended chain of about 3500 Å. Such a size is outside the explored Q range; SAXS data were therefore fitted with an "infinite cylinder" model, with an electron density fixed to its calculated value (0.43 e/Å^3). The value of the radius of the cylinder turns out to be 3.2 ± 0.1 Å, compatible with the cross dimension of the saccharide unit.

Nanoparticles. As remarked before, NCL80 and NCL20 SAXS data require only an instrumental background subtraction, while in the NCL5 case the scattering contribution of the residual chitosan molecules in solution has to be properly subtracted. The result of this subtraction is shown in Figure 6: the minimum at low Q values before the diffraction peak is more pronounced, and the scattering profile on both sides of the peak maximum is more symmetric with an overall shape similar to that of other vesicle suspensions.[41,42]

SAXS data for the NCL samples have been analyzed using eq S.3 (Supporting Information). The electron scattering densities of the lipid heads and tails were kept fixed to the values obtained for pure lecithin vesicles, reported in Table 3. The SAXS curves and the fits are shown in Figure 7 for the three chitosan/lecithin ratios investigated. The right panel shows the electron density profiles for each repeating unit (bilayer + half-interlayer on both bilayer sides). For the high-order multilayer contribution (represented by the g_4 number fraction in Table 3) the number of layers, N, depends on the chitosan/lecithin ratio: NCL5 and NCL20 data can be fitted with $N = 7$, while NCL80 requires an additional small contribution of $N = 11$ multilayers.

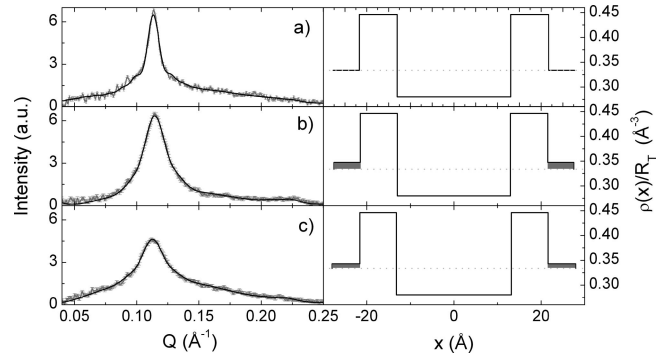

Figure 7. Left panel: SAXS curves for NCL80 (a), NCL20 (b), and NCL5 (c) samples showing the peak due to the multilamellar repetition. The continuous curves show the fit to eq S.3 (Supporting Information). Right panel: Electron density profiles derived from the fits. The gray area represents the interbilayer region occupied by water and chitosan.

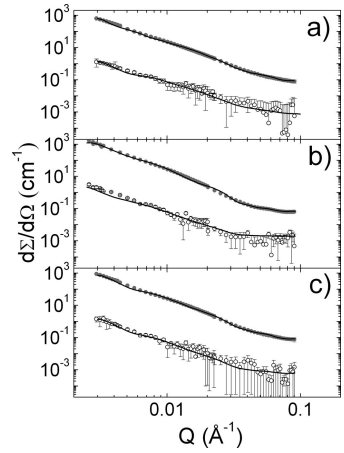

Figure 8. SANS curves of NCL80 (a), NCL20, (b) and NCL5 (c) samples in a perdeuterated solvent (full symbols) and in a solvent at the lecithin match point (open symbols). Data are shown after subtraction of a flat incoherent background. The curves obtained from the fit to eq S.5 (Supporting Information) (solid line) are also shown.

The diffraction peak of NCL80 is narrower than that of NCL5 and NCL20, indicating the presence of higher order multilayer repetitions, although in a very low number fraction. The diffraction peaks of NCL5 and NCL20 are similar in width but different in intensity; this can be attributed to different amounts of higher contrast chitosan in the interbilayer regions. In fact, the highest scattering length density of this region, ρ_{cw}, occurs in NCL20 samples, while it is lower for NCL5 and close to the solvent value for NCL80. In the explored Q range, a second-order diffraction peak should also be expected. It is indeed visible, but with a very low intensity, in the NLC20 curve at $Q \approx 0.22$ Å^{-1} (see Figure 7). This is due to the fact that, at the corresponding Q value, the form factor $P(Q)$ is close to zero.

SANS Data. Nanoparticles. The SANS experiments covered a Q range from 1×10^{-3} to 1×10^{-1} Å^{-1}, therefore extending the region explored with SAXS and providing information on the overall shape of the nanoparticles and on their size distribution. At low Q the influence of the nanoparticle clusters, like those observed in the cTEM micrographs (see Figure 1) and in the DLS data (see Figure 3), becomes important. Therefore, the SANS curves were analyzed only above $Q = 3 \times 10^{-3}$ Å^{-1}. In this region the NCL5 and NCL80 curves are well described by eq S.5 (Supporting Information) (Figure 8a,c); the NCL20 data still show some deviation at low Q values (Figure 8b) probably due to a residual contribution from large clusters (size >2000 Å). To

Table 4. NCL Samples: Parameters Obtained from the Fit of SANS Data According to Eq S.5 (Supporting Information)[a]

	NCL80	NCL20	NCL5
$\langle R_C \rangle$ (Å)	380 ± 8	350 ± 20	350 ± 10
σ	0.33 ± 0.04	0.5 ± 0.2	0.35 ± 0.02
α	0.04 ± 0.02	0.17 ± 0.02	0.15 ± 0.03
g_1 ($N = 1$)	0.67 ± 0.06	0.30 ± 0.01	0.6 ± 0.1
g_2 ($N = 2$)	0.10 ± 0.05	0.22 ± 0.01	0.13 ± 0.05
g_3 ($N = 3$)	0.18 ± 0.01	0.38 ± 0.01	0.20 ± 0.04
g_4 ($N > 3$)	0.02 ± 0.01	0.1 ± 0.1	0.05 ± 0.01
	($N = 11$)	($N = 7$)	($N = 7$)

[a] The values obtained for the core radius $\langle R_C \rangle$ and polydispersity σ are in agreement with those derived from statistical analysis of the cTEM micrographs.

obtain information on the location of chitosan within the nanoparticle, measurements were performed in two solvent buffers [(a) 100% D_2O and (b) 4/1 H_2O/D_2O] and almost match the coherent scattering length density of lecithin, ρ_B. The scattering contrast of chitosan, $\Delta\rho_{chitosan}$, has been calculated for both solvents, taking into account that three hydrogens (from hydroxyl and aminic groups) can be exchanged with deuterium from the solvent. During the fit, the parameters related to the bilayer structure, i.e., the thickness $t_B = 2(t_t + t_h)$ and the periodicity $d = t_B + t_{cw}$, were kept fixed to the values obtained from the SAXS data. The fit parameters in eq S.5 (Supporting Information) were therefore the mean core radius $\langle R_C \rangle$, its polydispersity index σ, the chitosan volume fraction α, and the number fractions g_i, with $\sum_i g_i = 1$. A combined fit of the SANS curves in the two solvents was performed for each nanoparticle species. The results are shown in Figure 8, and the obtained parameters are summarized in Table 4.

Discussion

The SAXS data indicate that the outer shell of the Lipoid vesicles is mostly made from single bilayers: multilamellar structures contribute only with $N \leq 3$. The structural parameters of the bilayers (head and tail thicknesses), as well as the scattering length densities, are in agreement with typical values for phosphocholine molecules.[43] Similar values are also found for the lipid/polysaccharide nanoparticles; their structure differs however from that of Lipoid vesicles since they show a pronounced multilayer structure (up to $N = 11$), with a periodicity of about 55 Å. This result is in agreement with a recent SAXS investigation on chitosan/lecithin nanovesicles in which high contents of multilamellar structures have also been observed.[44] The SAXS analysis is confirmed by the SANS data, which provide information on the overall nanoparticle shape and size distribution: the SANS values of $\langle R_C \rangle$ and σ agree well with those derived from the analysis of the cTEM images. Furthermore, it is possible to convert the number-weighted size distribution obtained from SANS to an intensity-weighted one, dividing the former by a suitable particle form factor (in the present case we adopted the form factor of a hollow sphere). The intensity-weighted distributions thus obtained have been analyzed with the cumulant method, and the results have been compared with those obtained from DLS at a fixed Q value (2.3×10^{-3} Å^{-1}). The comparison shows a reasonable agreement of the average radii for all the investigated samples as shown in Table 5.

On the basis of the SAXS and SANS scattering contrasts, as well as the colorimetry data, one can evaluate the chitosan to lecithin ratio per nanoparticle (C/L (w/w)). The values obtained from the three techniques are in good agreement as shown in Figure 9.

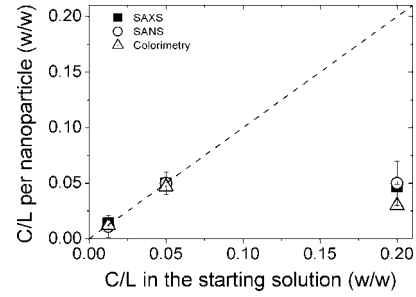

Figure 9. Chitosan/lecithin ratio, C/L, per nanoparticle determined from scattering and colorimetry measurements vs C/L in the starting solutions. Colorimetric data (open triangles), SAXS data (full squares), and SANS data (open circles) are in good agreement within the experimental accuracies. The dashed line corresponds to a full chitosan complexation within the nanoparticles.

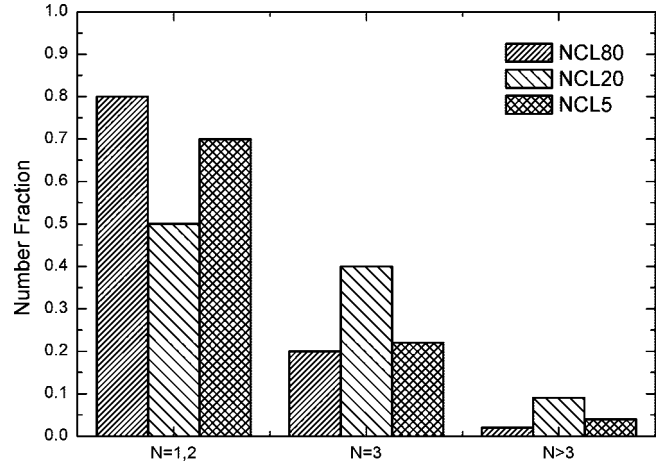

Figure 10. Number fraction of nanoparticles with different layer multiplicities, as determined from SANS.

Table 5. Hydrodinamic Radii Obtained by DLS and by Rescaling the SANS Number-Weighted Distributions

	NCL80	NCL20	NCL5
DLS radius (Å)	1140 ± 50	650 ± 20	570 ± 20
SANS radius (Å)	820 ± 80	650 ± 20	640 ± 10

It turns out that the amount of chitosan that can be complexed by Lipoid within the nanoparticle is limited, although exceeding charge neutralization. In fact, addition of chitosan beyond a 20/1 Lipoid/chitosan weight fraction results in increasing amounts of free chitosan in solution. It is worth noting that particles with a low number of multilayers predominate in formulations where positive and negative charges are not balanced; this is the case for NCL80 and NCL5 samples in which the nanoparticles are far from the point of charge inversion. In the case of NCL20 samples, where the amount of chitosan per nanoparticle is close to the limit of complexation, the number of particles with high layer multiplicity ($N \geq 3$) is higher as reported in Figure 10.

Chitosan complexation during nanoparticle assembly increases the particle size (more than 5-fold) and induces formation of higher order multilayer structures. The 20/1 system is the one closest to the charge inversion region (50/1 to 30/1 range, where macroscopic precipitation of the nanoparticles is observed).[5] This composition lies in the redissolution region, on the higher chitosan side, which is characterized by the re-entrant condensation

(43) Balgavý, P.; Dubnicková, M.; Kucerka, N.; Kiselev, M. A.; Yaradaikin, S. P.; Uhríková, D. *BBA—Biomembranes* **2001**, *1512*, 40–52.
(44) Mertins, O.; Sebben, M.; Pohlmann, A. R.; da Silveira, N. P. *Chem. Phys. Lipids* **2005**, *138*, 29–37.

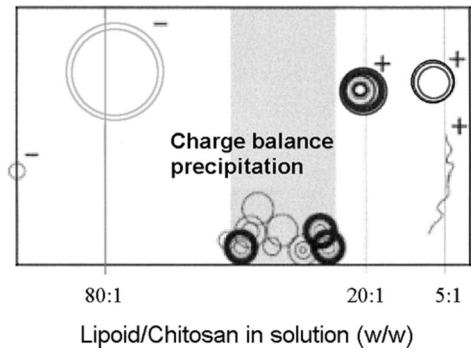

Figure 11. Pictorial sketch of the phase diagram of the Lipoid/chitosan system.

effect.[45,46] Indeed, for this composition clusterized nanoparticles have been observed with both cTEM and dynamic light scattering. The behavior of the nanoparticle system resembles that observed for vesicles with a polyelectrolyte cover, where, near the charge inversion region, a maximum in the coordination is observed at the mesoscale. In our case, since the sample preparation procedure allows for a close interaction between lipid and chitosan during nanoparticle formation, we detect a maximum in the coordination at the nanoscale. Close to the charge inversion region, a larger number of nanoparticles with a higher number of layers and a higher amount of chitosan per layer is formed. A pictorial sketch of the phase diagram is reported in Figure 11.

Conclusions

Lipid/saccharide nanoparticles made up of lecithin, a mixture of different lipids, and chitosan are of potential pharmaceutical interest. Their complexity, at the molecular level, is higher than that of particles made up of single lipid species. In spite of that, it has been shown here that, by applying complementary advanced techniques (DLS, cTEM, SAXS, and SANS), it is possible to describe the particle structure and morphology with satisfactory detail. The nanoparticles are characterized by a hollow core (typical size ∼700 Å), occupied by the aqueous solvent, surrounded by a multilayer structure made up of lipid bilayers and interlayer regions containing water and chitosan. The overall particle size ranges from ∼1100 to ∼2200 Å depending on the number of bilayers. Three different chitosan/lecithin ratios have been investigated. In the preparations with a lower chitosan/lecithin ratio (1/80, 1/20) all the chitosan present in the starting solution takes part in the nanoparticle structure. In the chitosan richer composition (1/5) only about 20−30% of the starting chitosan is found within the nanoparticles. The 1/20 composition leads to nanoparticles with the highest drug loading efficiency; this may be related to the presence of a large population of particles with a high content of multilamellar structures. We point out that multilamellarity could also play a control role in the kinetics of drug release since a higher number of confining layers has to be crossed (or dissolved). In this view a fine-tuning of the multilayer structure could play a key role in optimizing nanoparticle properties.

Acknowledgment. We are grateful to Dr. Göran Karlsson (University of Uppsala) for the cryo-TEM measurements. We also thank Dr. T. Narayanan and Dr. E. DiCola for their precious assistance on the ID02 beamline at ESRF. Financial support by the Ministry of University and Research (PRIN founding framework) is gratefully acknowledged.

Supporting Information Available: Mathematical derivations of the models used in this work to analyze DLS, SAXS, and SANS data and the full list of the model parameters together with their physical meaning. This material is available free of charge via the Internet at http://pubs.acs.org.

LA801992T

(45) Nguyen, T. T.; Rouzina, I.; Shklovskii, B. I. *J. Chem. Phys.* **2000**, *112*, 2562.
(46) Hsiao, P. Y. *J. Phys. Chem. B* **2008**, *112*, 7347–7350.